World Electric Vehicle Journal

MDPI

Article

Reduction in Measurement Time in Electrochemical Impedance Spectroscopy for Efficient Diagnosis of Batteries and Fuel Cells in Dynamic Vehicle Applications

Nicolas Muck [1,*] and Sebastian Esser [2]

[1] Department of Vehicle Energy Concepts, DLR-Institute of Vehicle Concepts, German Aerospace Center (DLR), Pfaffenwaldring 38-40, 70569 Stuttgart, Germany
[2] Department of Electrical Engineering, University of Stuttgart, Pfaffenwaldring 47, 70569 Stuttgart, Germany
* Correspondence: nicolas.muck@dlr.de

Abstract

This paper presents an innovative approach to modified electrochemical impedance spectroscopy (EIS) for real-time health monitoring of galvanic cells, particularly batteries and fuel cells in high-dynamic applications such as vehicles. Traditional methodologies, including cell voltage monitoring, offer limited diagnostic value. In contrast, conventional EIS provides comprehensive system insights; however, its applicability is constrained by prolonged measurement durations, rendering it impractical for dynamic conditions. This article presents a method that iteratively selects specific frequency bands and key points, thereby substantially reducing measurement time without compromising critical system information. This approach was initially validated using battery systems, which exhibit well-regulated operational behavior, thus facilitating a rigorous evaluation of the concept. Experimental results demonstrated that the modified EIS method achieves performance comparable to conventional EIS but with measurement times reduced by up to 92%. This validation underscores its reliability and precision, thereby supporting proactive maintenance strategies and extending system longevity. The reduction in measurement time enables more precise analyses across diverse dynamic operational spectra. Consequently, this approach constitutes a robust solution for health monitoring of fuel cells and batteries in dynamic environments, capitalizing on the advantages of EIS while addressing its inherent limitations.

Keywords: electrochemical impedance spectroscopy; health monitoring; fuel cells; batteries; high-dynamic applications; measurement time reduction; equivalent circuit model; proactive maintenance; lifecycle forecasting; dynamic environments; frequency selection

Academic Editor: Grzegorz Sierpiński

Received: 4 December 2025
Revised: 3 February 2026
Accepted: 5 February 2026
Published: 9 February 2026

1. Introduction

Current research in the field of fuel cells focuses on developing technologies that reduce costs for expensive materials such as catalyst layers and extend the lifespan of fuel cell stack components. Particularly critical in this regard is the membrane-electrode assembly. The introduction of cost-effective and large-volume manufacturing processes is also crucial for fuel cell systems to compete with traditional technologies [1].

Proton exchange membrane fuel cells (PEMFCs), which are currently used primarily in mobile fuel cell applications, efficiently convert the chemical energy of the fuel into electrical energy without relying on combustion or requiring a working medium. Thus, their energy conversion is not restricted by the Carnot cycle. Compared to batteries and internal

combustion engines, PEMFCs excel in energy efficiency and environmental sustainability. PEMFCs boast higher energy conversion rates—over 50% versus approximately 30–40% for internal combustion engines—and produce primarily water vapor, minimizing pollutant emissions. Their operational flexibility spans a broad range of temperatures and loads, making them suitable for a variety of applications. Recent technological improvements have enhanced their durability and longevity. Unlike batteries, which face challenges such as limited lifespan and slow recharging, PEMFCs continually generate electricity when fueled. Additionally, unlike internal combustion engines that burn fossil fuels, PEMFCs reduce greenhouse gas emissions and increase energy conversion efficiency. Ongoing research aims to boost cost-effectiveness, durability, and fuel diversity, positioning PEMFCs as promising candidates for sustainable energy solutions [1–3].

Furthermore, effective regulation of operating parameters within a fuel cell stack plays a central role in further improving this technology [1].

The demand for competitiveness of fuel cell systems is gaining increasing importance, especially against the backdrop of political requirements and user demands. Governments and system operators set clear targets for the lifespan of fuel cells to compare them with the lifespan of conventional power generation technologies, such as drive solutions in long-haul trucks or regional trains [4]. Currently, vehicle fuel cells achieve approximately 8000 to 25,000 operating hours in these dynamic usage environments, depending on operational requirements and conditions. In contrast, passenger cars typically have lower operating hours due to less intensive use patterns. Political and industrial goals for heavy-duty transport aim for a lifespan of at least 30,000 h [4,5].

To evaluate the lifespan of fuel cells in vehicles, driving performance or mileage and operating hours within their lifecycle are frequently used. Assuming an average speed of 60 km/h [6], which corresponds to a 40-ton truck for freight traffic on a typical route with sections of motorways and rural roads, the following conversion applies: At 10,000 operating hours, the maximum driving distance is 600,000 km; at 25,000 operating hours, it is 1,500,000 km; and the politically set target of 30,000 operating hours corresponds to a maximum driving distance of 1,800,000 km. These values must be considered in the context of the achieved mileage of conventional diesel trucks. Practical data show that heavy long-distance trucks typically reach a service life between 1,000,000 and 1,600,000 km. Converted into operating hours, this means about 16,667 operating hours for 1,000,000 km, and 1,600,000 km corresponds to about 26,667 operating hours [7].

Robust fuel cells for trucks, which also operate under optimized conditions, today fall within the same order of magnitude as the mechanical lifespan of diesel trucks and engines [8]. However, this assessment needs to be interpreted cautiously due to the currently still limited database, since most fuel cell vehicles are still in pilot and field test phases. Moreover, available field data indicate that most of the fuel cell systems examined so far have operating times in the lower range of the documented lifespan interval [9]. Thus, fuel cells are becoming increasingly competitive but are not yet at the same level as conventionally powered trucks [8]. The reason for this lies in the realistic assumption that the current lifespans of fuel cell units in actual fleet use have not yet attained the average level of conventional diesel engines, even though an increasing convergence can be observed.

With the requirement to further improve fuel cell systems, optimizing the efficiency, lifespan, and reliability of these systems constitutes a central area of research. Developments aimed at increasing efficiency are based both on optimizing cell materials, system architectures, operating conditions, and operating strategies [1,10] as well as approaches to enhance the overall system's efficiency, for example, through the use of metal hydride refrigeration machines [11] or hydrogen expansion machines [12–14].

For optimizing the system regarding lifespan and reliability, a comprehensive understanding of the current system state is essential to identify potential improvements and ultimately implement them. Detailed health monitoring for fuel cells enables proactive response to changes in conditions and thus maximizes the efficiency and lifespan of these components. It can also contribute to early detection of defects that cannot be compensated by an adaptively controlled mode of operation.

In modern applications, particularly in vehicular use, fuel cells, as well as batteries, are often considered "black box" systems because their internal states, apart from cell voltages, are difficult to monitor. Current health-monitoring methods such as cell voltage monitoring (CVM) in real deployment environments therefore exhibit significant limitations because they only capture data on cell, cell group, or total system voltage, providing statements about overall performance but no information about the causes of potential malfunctions [15].

The presently employed CVM in battery and fuel cell (FC) vehicles captures the voltages, compares them with defined minimum or maximum values, and signals when these threshold values are exceeded or fallen below. Additionally, CVM allows measuring cell voltages as a function of time, current, or other independent variables such as temperature, airflow rate, or humidity [16]. The voltage measurement data are recorded via a multichannel analog-to-digital converter with a typical sampling rate of 3–6 kHz. The resulting digital signal is transmitted, for instance, via CAN bus to the measurement system and converted by a monitor controller [17]. CVM has established itself as a standard and is used by all battery and FC system manufacturers. Nevertheless, there are variations in both placement and number of sensors used [18]. Continuous monitoring of each individual cell in the battery pack or FC stack is technically very demanding. Instead, equipping individual cells or cell groups at critical, heavily loaded positions with sensor technology seems more reasonable. For example, the CVM system currently deployed in FC vehicles frequently measures voltages using groups of several cells at both end regions of the stack and additionally in the middle of the stack.

The method presented in this work is intentionally designed to be measurement-data-driven and model-agnostic. Physics-based voltage models, which rely on CVM measurements, can indeed provide detailed insights into the causes of voltage deviations but require assumptions, parameterization, and system knowledge. Therefore, extracting characteristic measurement quantities robustly, without prior fault cause analysis and derivation, is preferable. Accordingly, model-based methods and the electrochemical measurement techniques discussed throughout this work are not directly comparable.

Current works on the lifespan and remaining useful life prediction of PEMFC encompass model-based approaches such as hybrid prognostic models [19], data-driven deep-learning approaches [20,21] and voltage-based health indicator models [21]. The integration of physics-based models to enhance error allocation is addressed later.

However, the CVM technology exhibits some limitations. When a malfunction is detected, the total voltage cannot specify the exact position or defective cell. Only monitoring every single cell could enable precise cell-resolved localization of defective cells. Regardless of the number and arrangement of voltage sensors, the fundamental problem of determining the cause of detected errors remains. From the voltage value of a cell, the cause cannot be derived if there is an unusual voltage drop. Therefore, the basis for optimization of operating conditions adapted to the current system status of the battery or FC through adjusted control strategies is missing.

These described factors cannot be recognized by CVM systems but play a significant role in the degradation and lifespan of the battery or FC. Hence, the further goal is to inves-

tigate alternative or potential measurement methods and procedures for more informative monitoring during vehicle operation.

Outside dynamic and real battery and FC applications, for example, in research and development of new cell generations and system architectures or quality assurance within the cell production process, measurement methods with the required accuracy and informativeness indeed exist. These methods are either impractical in terms of measurement effort or require stable operating points rarely present in the dynamic conditions of vehicle operation. Many existing procedures are also time-consuming and thus impractical for use under real driving conditions [22].

One of these methods is electrochemical impedance spectroscopy (EIS), which represents a highly precise method for state monitoring but requires long measurement times and stable operating points during the measurement duration. These requirements contradict the dynamic conditions in vehicles, where quick reactions to changing operating parameters are necessary. Thus, there is an urgent need for reliable measurement methods that are both precise enough and fast enough to monitor the state of FC and batteries in real-time.

To realize this, a measurement method capable of determining the current state of the system during operation according to the aforementioned aspects is required. EIS, already mentioned earlier, has been identified as a suitable measurement method in preliminary analyses. However, this method has not yet been effectively applied for state determination in mobile applications during operation. Reasons for this primarily lie in the relatively long measurement duration (up to 90 min and longer) and technical equipment required to perform a measurement.

To meet these challenges, the DLR Institute for Vehicle Concepts aims to develop a modified form of EIS to significantly shorten the measurement time of impedance spectroscopy and thereby enable its application in dynamically stressed environments, particularly in battery-electric and FC-powered vehicles. This allows for early detection of aging processes and defects, enabling efficient planning of maintenance intervals and avoidance of costly repairs. Moreover, accurate state information contributes to developing adaptive operating strategies that increase energy efficiency and minimize environmental impact.

In EIS, enhancing measurement robustness and enabling quantifiable estimates are crucial. Adaptive frequency reduction shortens measurement times, approximates stationary conditions more closely, and enhances robustness against load fluctuations.

This work aims to achieve a data-driven reduction in the necessary EIS frequency points through algorithmic selection of relevant frequency ranges. Therefore, the focus lies exclusively on the software-based optimization of frequency selection and does not address hardware-related acceleration of signal acquisition.

There is no claim that aEIS replaces a comprehensive EIS entirely. Instead, there is an application-oriented trade-off between measurement time and informational density. Adaptive frequency selection positions itself as a complementary approach tailored for dynamic applications, offering a balanced solution that optimizes efficiency without compromising essential data integrity.

The structure of this work has been deliberately designed to clearly emphasize the relevance and lack of viable alternatives to accelerated EIS in the context of condition monitoring of fuel cells and batteries in automotive applications. Section 2 examines the application of electrochemical measurement methods for characterizing and evaluating galvanic cells, focusing specifically on EIS. Direct and indirect approaches are compared to determine performance parameters and the state of the cells. Section 3 describes the methodology of modified impedance spectroscopy, including the development approach, principles of EIS, and integration into measurement techniques and testing systems. Section 4 addresses

the experimental setup and implementation of measurement technology in the fuel cell test bench. Section 5 presents the measurement results, and Section 6 discusses them. Finally, Section 7 summarizes the findings, draws conclusions, and provides an outlook on future research.

2. Related Work

The current state of the art and research in the field of state detection of galvanic cells encompasses a variety of electrochemical measurement methods. This section will show why EIS is nearly indispensable due to its ability to analyze various degradation processes in detail. Simultaneously, the limitations of the method, particularly the long measurement durations and the necessity of stable system operation, will be highlighted. Finally, it will be explained why shortening the measurement duration is essential to effectively employ EIS in dynamic operating environments of batteries and FC as a State of Health (SoH) monitoring system. The dynamic load requirements of vehicular applications impose constraints on conventional EIS measurements, necessitating that the fuel cell operate at a steady-state condition. However, maintaining such stability is often impractical within the fluctuating operational environment of vehicles. Therefore, it is imperative to significantly reduce the measurement duration of EIS to align with the transient steady-state intervals experienced by the fuel cell during actual driving conditions.

The objective of electrochemical characterization is to gain both quantitative and qualitative insights into electrochemical processes, such as those occurring at electrode-electrolyte interfaces and within electrode materials [23]. This enables a comprehensive evaluation of performance parameters like capacity, internal resistance, aging, and efficiency of galvanic cells [24].

The underlying principle of the employed measurement methods involves applying a defined electrical stimulus, such as a current or voltage signal, and analyzing the system's response [24]. These responses can include voltage profiles or impedance spectra. By evaluating these data, transport processes, kinetic events, and thermodynamic states crucial for understanding the functioning and performance can be deduced.

Another important aspect is examining different operating states and their dynamics, distinguishing between steady-state and transient conditions, the latter being characterized by rapid changes in operating behavior [25]. Since most FC and battery systems used in real-world applications experience semi- and full-dynamic stresses, the development of advanced and operando-capable measurement methods is indispensable.

2.1. Direct Measurement Methods for Quasi-Realtime SoH in Dynamic System Operation

Direct measurement methods differ from indirect ones by allowing the measurability of physical and electrochemical characteristics. This enables immediate derivation of the SoH of the system being investigated. Focus is placed on characteristics such as capacity, internal resistance, impedance, conductivity, and charging efficiency, which can either be directly measured or determined through simple calculations. These methods exhibit minimal or no model/data dependency, enhancing the reliability and reproducibility of results [26]. Consequently, a robust and transparent evaluation of the system SoH is ensured, remaining independent of external parameters and assumptions [27].

Examples of direct methods in dynamically operated galvanic cells include EIS, along with its nonlinear and non-stationary extensions [27]. While EIS holds a special case that will be discussed later, other methods encompass Coulomb counting, direct-current internal resistance analyses, open-circuit voltage measurements, ultrasound, acoustic methods, and fiber-optic temperature and moisture measurements [27–30].

2.2. Indirect Measurement Methods in Dynamic System Operation

Indirect methods are not directly through measurable characteristics but rather through model-based or data-driven evaluation procedures [28,31]. The objective is to derive SoH-relevant parameters from measurement data by employing mathematical models or identification methods [28,32]. Data sources include current, voltage, temperature, and impedance data obtained from both real operation and targeted measurements [31,33]. A distinctive feature is that explicit SoH measurement does not occur. Instead, SoH is estimated or identified through model adaptation or signal processing [32,34].

Indirect methods comprise approaches such as Kalman filter-based models, equivalent circuit model parameter estimations, and data-driven methods based on machine learning architectures [25,35].

These methods will not be explored further here, as directly measurable electrochemical characteristics generally offer higher accuracy, reproducibility, and physical representativeness concerning the actual cell state. Nonetheless, indirect approaches remain valuable for predictive state monitoring and model-supported lifetime prognostics, especially when integrating measurement technology appears infeasible economically and technically [35].

2.3. Electrochemical Impedance Spectroscopy and Its Potential

The EIS serves as an interface between direct and indirect measurement methods, relying on directly measured current and voltage responses whose physical interpretation occurs model-assisted [34].

EIS is utilized in the chemistry of galvanic cells to characterize FC and batteries in situ, studying various processes such as mass transfer, charge transfer reactions at electrode/electrolyte interfaces, diffusion processes, and reaction mechanisms responsible for the relationship between current and voltage during operation. Through EIS, intrinsic material properties or specific processes influencing the conductivity, resistance, or capacitance of systems can be investigated. Compared to other diagnostic methods, EIS is relatively invasive and capable of differentiating various error types and identifying diverse causes of state deterioration [36].

Typically, a sine wave functions as the excitation signal in EIS, modulated onto a constant cell base load. The emerging response signal from the system differs in amplitude and phase relative to the excitation signal. This change can then be captured and interpreted by the measuring device [37]. Figure 1 schematically shows this as a specific operating point in a polarization curve of a fuel cell according to Wang et al. [38].

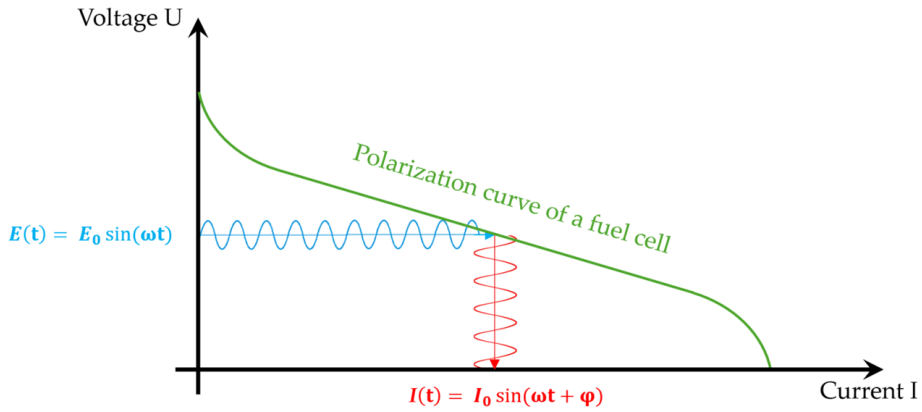

Figure 1. Schematic representation of the excitation and response signals of EIS.

For the impedance Z of a galvanic cell under investigation influenced by a periodic sinusoidal excitation voltage E_t over the system to be measured with alternating response signal I_t (see Figure 1), the following applies:

$$Z = \frac{E_t}{I_t} = \frac{E_0 \ \sin(\omega t)}{I_0 \sin(\omega t + \varphi)} \tag{1}$$

where E_0 is the voltage amplitude, I_0 is the current amplitude, ω is the angular frequency at observation time t, and φ denotes the phase angle between voltage and current [39]. The time-dependent relationship from Equation (1) can be transformed into a frequency-dependent function via Fourier transformation as per [40]:

$$F(\omega) = \int_{-\infty}^{+\infty} f(t) e^{-j\omega t} \, dt \tag{2}$$

Thus, the impedance at a particular frequency, related to $\omega_i = 2\pi f_i$, can be expressed as:

$$Z(\omega) = \frac{\widetilde{V}(\omega)}{\widetilde{I}(\omega)} \tag{3}$$

Both quantities can be described by complex phasors $\widetilde{V}(\omega)$ and $\widetilde{I}(\omega)$, which represent the amplitudes and phase angles of the harmonic signal components. The frequency-dependent impedance results from the ratio of the voltage phasor to the current phasor, both of which are complex time-invariant numbers accounting for the amplitude and phase of a sinusoidal function. Since $Z(\omega)$ is inherently a complex quantity, the tilde notation is typically omitted. Converting to polar form and simplifying yields:

$$Z(\omega) = \left| \frac{\widetilde{V}(\omega)}{\widetilde{I}(\omega)} \right| (cos\varphi(\omega) + jsin\varphi(\omega)) = Z' + jZ'' \tag{4}$$

where j signifies the imaginary unit with $j = \sqrt{(-1)}$. Electrochemical impedance can hence be represented as a frequency-dependent complex quantity, with the real part Z' corresponding to the resistive component and the imaginary part Z'' corresponding to the frequency-dependent reactive component [41].

The expression $cos\varphi + jsin\varphi$ from Equation (4) corresponds to Euler's formula $e^{j\varphi} = cos\varphi + jsin\varphi$. This mathematical formulation permits compact representation of sinusoidal signals in the frequency domain and forms the basis for utilizing phasors. Transforming into the frequency domain allows electrochemical processes to be determined and analyzed separately as frequency-dependent contributions to the complex impedance [41].

For visualizing and analyzing EIS measurement data, two primary diagram types are mainly used: Nyquist and Bode plots. The Nyquist plot displays the imaginary part of the impedance versus the real part. Semicircles or other characteristic shapes in this plot correlate with various processes inside the galvanic cell. This plot facilitates differentiated examination of individual effects such as electrode reactions, gas diffusion, and membrane capacitance. Practically, the Nyquist plot aids in identifying degradation causes like catalyst aging or membrane damage [42]. The presentation of impedance in the Nyquist plot will primarily be used for subsequent discussions within this work. Conversely, the Bode plot shows the magnitude of the impedance $|Z|$ and φ over frequency. It suits observing frequency-dependent trends but is less intuitive for directly separating individual processes [36].

Given the initially defined goal of not only determining the current SoH of the system but also identifying potential disturbances and faults, EIS stands out as an almost unrivaled method.

Nevertheless, there are substantial challenges. EIS necessitates a stable system configuration. During measurement, the fuel cell must operate constantly, requiring control over temperature, pressure, and humidity. Additionally, measurement durations are relatively lengthy. The long measurement times associated with conventional EIS can be attributed to several physical causes rooted in the relationship between low frequencies, extended period durations, and the relaxation time constants of electrochemical processes. At lower frequencies, typical processes such as mass transport/diffusion, water transport within the membrane, and slow electrochemical relaxations become prominent. These phenomena have inherent time constants that necessitate longer periods for complete characterization [15,41]. However, it is important to clarify that not all relaxation processes are equally relevant for every target parameter. Dominant relaxations manifest themselves in characteristic frequency ranges [24]. Consequently, fully scanning the low-frequency range mandates prolonged measurement times, which becomes particularly critical under non-stationary operating conditions where rapid changes occur [15,41]. Furthermore, EIS is sensitive to external interferences such as noise and temperature fluctuations.

It is crucial to differentiate between the hardware level and the algorithmic level in addressing the challenges of conventional EIS. On the hardware side, efforts focus on accelerating signal acquisition. In contrast, at the algorithmic level, the aim is to reduce the number of required excitations. Both approaches tackle different bottlenecks in conventional EIS: hardware improvements enhance the speed of data collection, while algorithmic refinements optimize the efficiency of data usage. As they address distinct aspects of the problem, these two strategies can be combined synergistically without methodological conflicts, leading to a more robust and efficient impedance spectroscopy framework.

These limitations underline the core issue: prolonged measurement times of conventional EIS restrict practical applicability in dynamic uses and continuous monitoring. There is thus a pressing motivation to accelerate EIS methods without sacrificing diagnostic insight. Subsequently, a method will be introduced to shorten measurement duration while retaining resolution of individual degradation mechanisms.

The methodology outlined herein concentrates on expediting the frequency-based measurement process while preserving the plausibility of the collected data across multiple measurement series. The analysis of EIS measurement data traditionally employs an equivalent circuit model, which is likewise utilized in this study. Consequently, the exploration of alternative models for data evaluation falls outside the view of this research.

3. Methodical Approach

This section presents the methodological approach for performing accelerated EIS (aEIS) on a lithium-ion battery cell. The goal is to develop an adaptive concept for reducing measurement time, enabling precise and efficient capture of electrochemical processes within the cell. The core of the methodology involves selecting relevant frequency ranges based on model-supported parameter analyses, significantly shortening the measurement duration without losing diagnostic insight.

3.1. Development Approach

The focus of this paper is on developing and validating a methodology for accelerated acquisition of EIS using a lithium-ion battery cell as a model system. Although the long-term goal is to apply aEIS to SoH analysis of FC under real operating conditions, the battery

offers a suitable platform for systematic investigation of measurement and evaluation methodologies due to its stable and well-controlled operating behavior.

The objective of the methodology is to substantially reduce measurement duration without compromising diagnostic insight. This is achieved through adaptive frequency selection concentrating on frequency ranges relevant to describing electrochemical processes, combined with model-based evaluation procedures ensuring physically consistent data interpretation [43,44]. The methodological approach includes conceptual development, implementation, and experimental validation. Results obtained from the battery cell serve as the foundation for transferring the methodology to FC systems.

3.2. Modification of the Conventional EIS

The steps illustrated in Figure 2 constitute the methodological framework of the developed procedure for adaptive measurement time reduction. The methodology comprises preparatory steps for system parameterization and the actual execution of adaptive measurement.

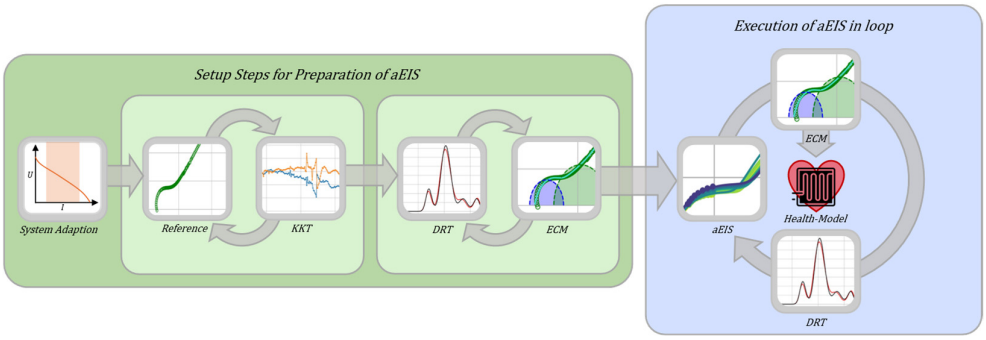

Figure 2. Methodology for Adaptive Measurement Time Reduction.

In the first part, the preparatory steps involve capturing a reference measurement validated for physical consistency using Kramers-Kronig transformations [45,46]. The quality of this reference measurement is critical, as it determines the ECM structure and characteristic frequencies that guide all subsequent adaptive measurements. If measurement data deviate from KKT conditions, operating parameters or measurement configurations are adjusted until the reference falls within defined tolerances. Based on these validated data, Distribution of Relaxation Times (DRT) analysis identifies characteristic electrochemical processes and their time constants [47]. Information gained serves as the basis for creating an Equivalent Circuit Model (ECM), whose parameters are determined through nonlinear fitting to the reference measurement. This model describes relevant subprocesses—such as conductivities, contact resistances, and diffusion-limited effects—and forms the basis for parametric mapping of cell behavior [47,48].

Nonlinear fitting uses the Levenberg-Marquardt algorithm with initial parameter estimates derived from graphical analysis and DRT peak positions. Physical constraints ensure positive resistances and inductances, time constants within electrochemically realistic ranges, and appropriately bounded CPE exponents. From the fitted ECM parameters, characteristic frequencies are calculated from their time constants, identifying spectral regions where processes contribute most significantly.

In the second part, executing the adaptive measurement selects frequency ranges relevant to ECM modeling. Only intervals derived from the model are captured in detail, while measurement point density is reduced in less model-relevant areas. The frequency grid comprises two components: fixed baseline points distributed logarithmically across the full frequency range with 2 points per decade in lower-resolution regions and 5 points per decade in higher-resolution regions, and adaptive cluster points concentrated around

each characteristic frequency. For the implemented ECM with two characteristic time constants (charge transfer and diffusion), measurement points are positioned around each characteristic frequency using frequency multiplication factors. These factors are selected to establish baseline values outside the transition region, capture the transition onset and completion, and provide fine resolution at the inflection point.

For diffusion processes, the frequency multiplication factors are selected to minimize the number of measurement points within the diffusion-dominated range. Since measurement duration per point increases significantly as frequency decreases, reducing the point density in this specific range offers the greatest potential for saving overall measurement time. To accurately capture the transition to the diffusion-dominated regime while ensuring high incremental information content, an additional measurement point is positioned at the local impedance minimum immediately preceding the diffusion branch.

The frequency grid continuously adapts to the current state of the electrochemical system. Parameters are fitted within physically plausible limits, and changes in time constants and resistances are detectable in real-time via DRT analysis. After each measurement cycle, the adaptive algorithm executes the following sequence: Measured impedance values are combined with ECM-predicted values at unmeasured frequencies to reconstruct a complete impedance spectrum. The ECM parameters are then refitted to this reconstructed spectrum using the previous cycle's parameters as initial estimates. New characteristic frequencies are calculated from the updated time constants, and the adaptive frequency clusters are automatically repositioned to maintain the measurement pattern around the shifted characteristic frequencies.

The reduced number of measurement points in aEIS limits Kramers-Kronig validation, as the lower sampling rate does not meet the frequency resolution requirements for reliable KKT analysis. While combining measured points with ECM-predicted values at unmeasured frequencies addresses the insufficient data density, this approach lacks independence since the ECM-generated impedances are inherently causal and linear by construction, guaranteeing KKT fulfillment regardless of whether the measured data satisfy the required conditions [45]. In tests with combined data, residuals were elevated at frequencies where actual measurements were performed. However, due to conceptual ambiguities in the validation of measured data within a predominantly model-generated spectrum, the authors decided against using KKT for aEIS data verification. Therefore, KKT validation is only applied to reference measurements. Residuals between measured points and ECM predictions are continuously monitored for quality assessment, though automated corrective actions based on residual thresholds could be implemented in future refinements of the methodology.

3.3. System Integration

The test bench architecture combines software and hardware components for automated and adaptive EIS measurements. The developed application integrates reference data, controls measurement procedures, and cyclically analyzes and stores measurement results.

Measurements are executed via a Python 3.13 interface on the used measurement system, consisting of the Zennium X and EL1000 load from Zahner-Elektrik (Kronach, Germany). Control is program-guided, including setting frequency range, current amplitude, and measurement strategy.

Regarding computational requirements, the aEIS methodology was validated on standard computing hardware, with computational overhead remaining well below measurement cycle duration, demonstrating compatibility with automotive electronic control units without specialized high-performance computing resources.

The EIS signal is applied in galvanostatic mode, where the optimal current amplitude is specified by systematically varying the parameters of the electrochemical target system. During this variation, linearity of the electrochemical response was verified by frequency domain analysis of the voltage response, ensuring that only first-order harmonic components were present without higher-order harmonics, while maintaining sufficient response amplitude above noise levels.

EIS measurement employs a 4-electrode system, where working and counter electrodes supply stimulation, and reference and sense electrodes capture voltage response. All cables are twisted and shielded, with impedance measurement and electrical test bench components galvanically separated to minimize interference.

3.4. Measurement Cycle and Strategy

Applying aEIS in a vehicle context requires a measurement strategy tailored to the dynamics of the electrochemical system. Given real driving conditions marked by continuous load changes, temperature fluctuations, and transient effects, conducting measurements under fully dynamic operating conditions is only partially feasible [49]. Therefore, the methodology focuses on periods exhibiting quasi-stationary behavior—for example, during standstill phases or constant power demand. Within these intervals, current, voltage, and temperature can be deemed sufficiently stable over measurement duration, ensuring physically consistent impedance data capture [50,51].

In the proof-of-concept study conducted as part of this work, quasi-stationary conditions (QSC) were ensured through several criteria. Before each measurement, a relaxation period was applied until the cell voltage had stabilized, ensuring that the system had reached a near-equilibrium state. During each accelerated EIS measurement, the voltage response was continuously monitored to confirm linearity, ensuring that the system operated within the linear range around the operating point and that the excitation amplitude was appropriate. At regular intervals, full-frequency EIS reference measurements were performed and validated using Kramers-Kronig relations to verify linearity, causality, and stationarity, thereby confirming the validity of the accelerated measurement approach. All measurements were conducted under controlled laboratory conditions with stable temperature and current setpoints. The definition of specific quantitative QSC criteria, such as permissible drift rates (dV/dt, dI/dt, dT/dt), is subject to ongoing research and may vary significantly depending on the electrochemical target system.

Under laboratory conditions, both stable and deliberately unstable operating phases are simulated to examine aEIS functionality and assess method boundaries during transient events. Though chosen scenarios diverge considerably from real vehicle conditions, they allow systematic investigation of measurement strategy under controlled and reproducible settings. While these quasi-stationary operating windows are well-justified, adhering to certain prerequisites for the measurements is necessary to obtain reproducible results. Rapid load transients can introduce significant fluctuations in electrochemical processes, potentially leading to inconsistencies in impedance measurements. Similarly, thermal gradients within the cell can cause localized temperature variations, affecting reaction kinetics and ion transport, which in turn influence the measured impedance. To ensure reliable and reproducible results, it is essential to maintain stable conditions during measurements.

Designing the measurement strategy and adaptively adjusting frequency selection and measurement time aligns with the target system's characteristics and electrochemical dynamics. This adjustment enables aEIS to balance temporal resolution and measurement precision flexibly according to system conditions.

The developed measurement cycle serves as the methodological starting point for experimental validation of the proof-of-concept. Subsequent investigations verify how

consistently and physically plausibly aEIS delivers results under defined stability levels and how shortened measurement duration impacts data quality.

4. Experimental Setup and Implementation

This section describes the experimental setup for implementing the developed aEIS methodology. The focus is on constructing and calibrating the test bench, defining measurement parameters, and performing and validating the reference measurement as the basis for subsequent adaptive application. The goal is to ensure the functionality, stability, and reproducibility of the system under controlled conditions.

4.1. Test Setup

Figure 3 illustrates the schematic layout of the test bench used for implementing aEIS. The system consists of a Zahner Zennium X (Kronach, Germany) potentiostat, a Zahner EL1000 (Kronach, Germany) electronic load, and a programmable climate chamber for thermal conditioning of the cell. Control and data acquisition are managed by the developed Python-based application, which automates measurement parameters, frequency grids, and data evaluation.

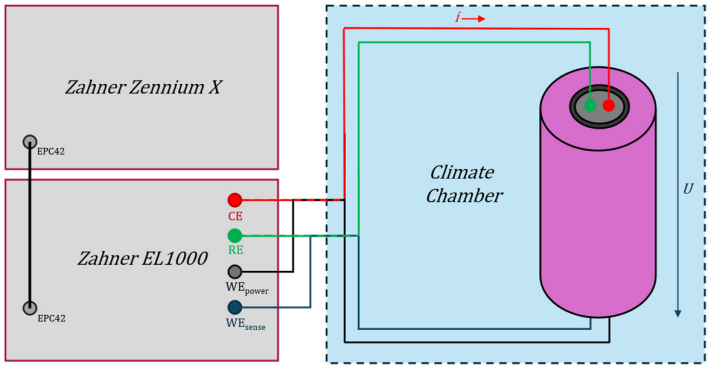

Figure 3. Layout of the Test Bench.

Measurements are conducted on a cylindrical 21700 lithium-ion cell with a nickel manganese cobalt oxide cathode and graphite anode. For validating aEIS, a commercial round cell is selected, whose electrochemical behavior is comprehensively characterized and documented in the literature [44,52,53].

The subsequent procedure follows the methodology described in Section 3, divided into a preparatory setup process and a subsequent loop process. This section focuses on the setup part, where the system's readiness and stability are verified, and the measurement strategy is prepared.

4.2. Procedure for Implementing the Methodology

The first step involves adapting aEIS to the target system, optimizing the measurement configuration for the electrochemical properties of the battery cell. Excitation amplitude, frequency range, and integration cycles are experimentally determined to ensure a stable signal-to-noise ratio and reproducible measurement conditions. The parameters obtained form the basis for all subsequent measurements and are summarized in Table 1.

Next, a comprehensive reference measurement is taken across the entire relevant frequency range of the target system to capture the detailed electrochemical behavior of the cell. This measurement is recorded at a stable operating point as a reference for further analysis. Validation of physical consistency is performed using the Kramers-Kronig transformation, checking linearity, time invariance, and causality. Analysis of residuals

ensures that both the real and imaginary parts of the impedance exhibit deviations well below the critical threshold of 0.5% throughout the frequency range [45,47].

Table 1. Measurement Parameters for Reference Measurement and aEIS.

	Reference Measurement	aEIS Measurement
Method	galvanostatic	galvanostatic
Excitation Amplitude	100 mA	100 mA
Frequency Range	0.07 Hz–3000 Hz	0.1 Hz–3000 Hz
Number/Type of Measurement Points per Decade	15 fixed	fixed + adaptive
Integration Cycles	3 (<66 Hz), 10 (>66 Hz)	3 (<66 Hz), 10 (>66 Hz)
Measurement Duration	677 s	60 s

Based on the validated reference data, a DRT analysis is conducted to identify characteristic time constants and electrochemical sub-processes [54,55]. From this, an ECM is derived, describing the dominant ohmic, capacitive, and diffusion-related effects of the cell [48,56]. Multiple ECM topologies were evaluated during method development, including simple Randles circuits, multi-Zarc configurations, and models incorporating different kinds of Warburg diffusion elements. However, the focus in selecting the ECM was not on detailing all electrochemical sub-processes of the cell but rather on representing the fundamental cell behavior for validating the applied methodology.

Figure 4 shows the resulting ECM, and Figure 5 validates it: Part (a) depicts the fit of the reference measurement in the Nyquist representation, and part (b) shows the corresponding DRT distribution.

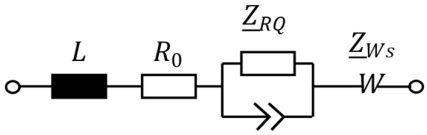

Figure 4. Chosen ECM for Modeling the Cell.

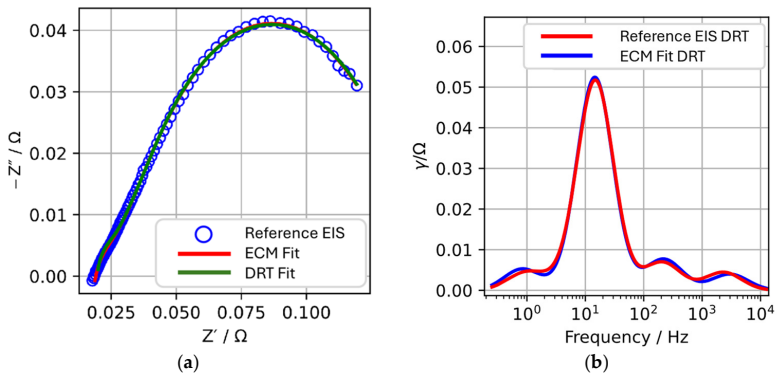

Figure 5. (**a**) Fit of the Reference Measurement using ECM and DRT; (**b**) DRT Distribution.

There is excellent agreement between the measured and modeled data in both Nyquist and DRT representations, confirming the physical consistency of the model. The ohmic resistance R_0 describes conduction and contact losses within the cell architecture and is sensitive to changes in the electrical resistance network, for example, due to temperature or aging. The R_{RQ} element models charge-transfer-limited processes at the electrode interfaces, whose behavior is strongly temperature-dependent as both reaction kinetics and ion transport are thermally controlled. The additional Q element captures diffusion-controlled processes in the low-frequency range, determined by mass transport in the electrolyte [48,53,56].

With the successful completion of the reference measurement, the Kramers-Kronig validation test, and subsequent model building, the setup process using the aEIS methodology is concluded. It confirms the measurement capability of the system and ensures that aEIS can be reliably applied under stable and reproducible conditions. On this basis, the next step involves the loop process, where adaptive frequency selection and measurement time reduction are implemented.

5. Results

This section describes the experimental investigation of the developed methodology. The goal is to evaluate its performance and applicability under various operating conditions. To this end, a multi-stage test sequence is carried out, in which measurement results are recorded over an extended period and compared with reference data.

5.1. Test Sequence

After successfully validating the reference measurement, the aEIS is tested within a long-term measurement loop. The purpose of this test is to examine the stability of aEIS over an extended period and under controlled temperature changes. The test sequence is divided into three consecutive phases. In Phase I (0–2000 s), measurements are taken at 20 °C room temperature without active temperature control. Phase II (2000–8000 s) involves heating the environment to 50 °C and actively controlling the battery cell's temperature. In Phase III (8000–15,000 s), the temperature control of the climate chamber is turned off, allowing the battery cell to cool down passively. Throughout the entire test period, continuous aEIS measurements are performed to detect changes in the cell's electrical behavior. Additionally, complete reference measurements are taken at the beginning of the test, after completing the temperature control phase, and at the end of the cooling phase.

In Figure 6, the green marked points in Figure 6b correspond to the respective active plots shown in Figure 6a. The time intervals mentioned in the figure captions refer to the respective Phase I–III temperature intervals.

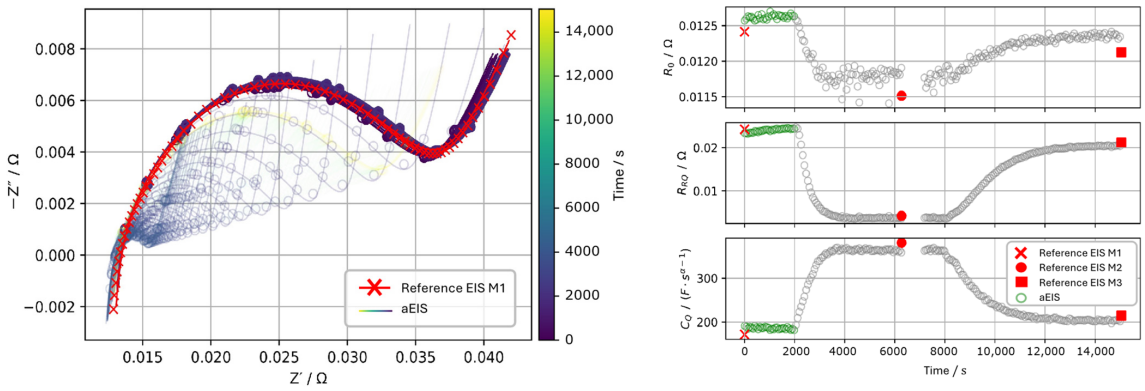

Figure 6. (**a**) Nyquist Plot of aEIS and Reference Measurement; (**b**) Temporal Evolution of Selected ECM Parameters from 0 to 2000 s.

Before the test sequence, the battery cell was first charged to a SoC of 50%. This was achieved by a CC-CV charging process to a target voltage of 3.7 V, which corresponds to the OCV of the cell at 50% SoC. After charging, the cell was relaxed for 6 h. During all subsequent test phases, the cell was excited exclusively by the AC amplifier without DC offset so that the SoC remained constant throughout the measurements.

5.2. Phase I

In Phase I, the battery cell is examined under stable ambient conditions at 20 °C room temperature. No active temperature control is applied in this phase; the cell is in the uniformly temperature-controlled air flow of the climate chamber. The goal of this phase is to verify that aEIS does not influence the electrochemical behavior of the battery cell and enables stable and reproducible parameterization.

Figure 6a shows the Nyquist plot of the impedance measurements from 0 to 2000 s. For better clarity, the considered time section is color-highlighted, while measurements outside this range are displayed transparently. The aEIS measurement results largely overlap with the separately recorded reference measurements. Neither in the high-frequency region, dominated by ohmic resistance, nor in the low-frequency region, characterized by charge-transfer and diffusion-limited processes, are there significant deviations [44,53]. This observation confirms that the reduced number of points in aEIS measurements does not cause information loss and that the electrochemical characteristics of the cell remain unchanged by aEIS.

To quantitatively validate this observation, impedance deviations between aEIS and the reference measurement were calculated at matching frequency points. The comparison at six fixed frequencies (901.8 Hz, 271.1 Hz, 81.5 Hz, 7.4 Hz, 2.2 Hz, and 0.2 Hz) reveals a mean impedance magnitude deviation of 1.01%, with a maximum deviation of 2.04% occurring at the lowest frequency.

The temporal evolution of selected modeled ECM parameters is depicted in Figure 6b. The extracted model parameters show high stability over the entire measurement period.

Comparison analysis with the reference measurement shows very good agreement of the parameters, confirming the validity of the model building based on aEIS measurements compared to the complete reference measurement.

For deeper investigation, a DRT analysis is performed, shown in Figure 7. There is a clear agreement between the results of aEIS and the reference measurement. The positions of the main peaks and their associated time constants remain stable throughout the period. Neither additional electrochemical processes nor significant shifts in the existing peaks are recognizable [47,56].

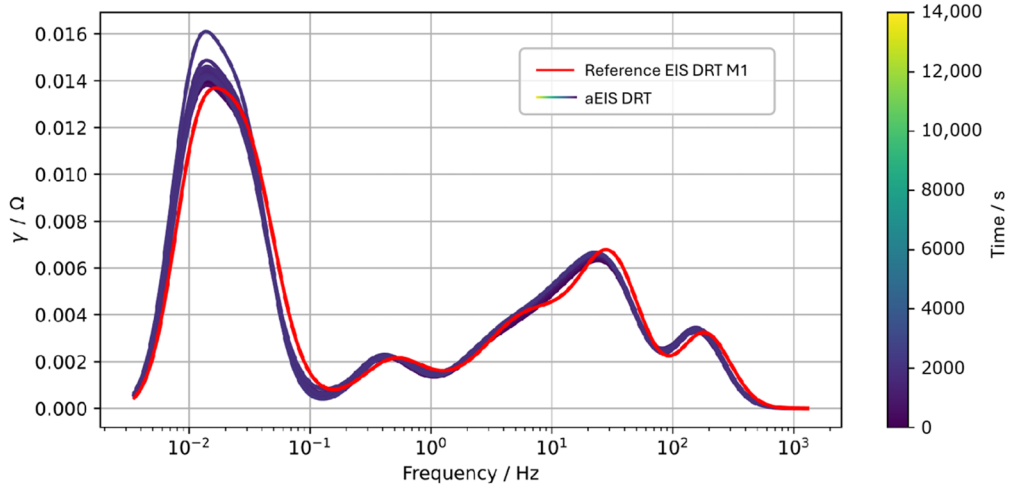

Figure 7. Comparison of DRT Analysis of aEIS and Reference Measurement from 0 to 2000 s.

5.3. Phase II

In Phase II, the battery cell is subjected to controlled temperature changes to study the effect of temperature variations on electrochemical behavior. Starting at t = 2000 s, the temperature in the climate chamber is set to 50 °C. Due to thermal inertia, the cell temperature gradually approaches the setpoint over several minutes. The goal of this

phase is to verify that aEIS delivers stable and reproducible measurement results even under dynamically changing temperature conditions and correctly captures temperature-dependent changes in electrochemical processes [44,53].

Figure 8a shows the Nyquist plot of the impedance measurements from 2000 to 8000 s. Compared to the room temperature phase (Phase I) and the reference measurement, the impedance curves shift noticeably to lower resistance values. The diameter of the semi-circle decreases, indicating a reduction in ohmic resistance R_0 and charge-transfer-limited resistance R_{RQ}. This behavior matches physical expectations, as increased temperature improves reaction kinetics and facilitates ion diffusion [43,53]. The aEIS measurement results largely overlap with those of the reference measurements, confirming that even under thermally varying conditions, no information loss occurs due to the reduced number of measurement points, and the electrochemical characteristics of the cell are accurately captured. Quantitative validation at matching frequency points shows even lower deviations during the temperature-controlled phase, with a mean impedance magnitude deviation of only 0.18% and a maximum of 0.38%.

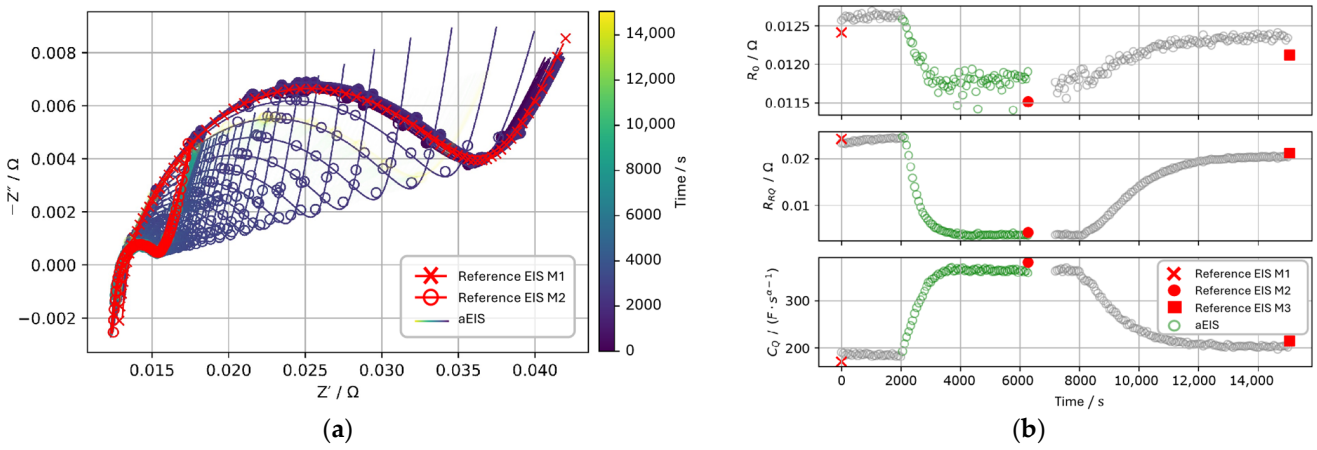

Figure 8. (**a**) Nyquist Plot of aEIS and Reference Measurement; (**b**) Temporal Evolution of Selected ECM Parameters from 2000 to 8000 s.

The temporal evolution of the modeled ECM parameters is depicted in Figure 8b. Over the considered period, a distinct decrease in R_0 and R_{RQ} is observable, matching the expected Arrhenius behavior of electrochemical processes: with rising temperature, activation energy decreases, leading to increased reaction rates [48,53]. Notably, R_0 in the heated state exhibits stronger scattering than R_{RQ}, suggesting higher sensitivity to local temperature gradients or contact fluctuations.

Simultaneously, the capacitance C_Q increases with rising temperature, attributable to improved ion mobility and enlarged effective double-layer capacitance [44,48]. Overall, the model parameters extracted from aEIS measurements agree very well with those from the reference measurements, confirming the validity of the model building. For further analysis, a DRT evaluation is performed, shown in Figure 9.

The DRT results show a shift of peaks to shorter relaxation times, indicating accelerated electrochemical processes due to temperature increase. Especially in the mid-frequency range between 10 Hz and 1000 Hz, resistive components decrease significantly, suggesting a lower activation barrier for charge-transfer-limited processes [47,56].

The calculated DRT courses of aEIS again match very well with the reference data, demonstrating the reliability of aEIS under altered thermal conditions. However, the peak in the low-frequency range, representing diffusion-limited processes, initially increases and subsequently decreases. This behavior cannot be clearly explained physically, as usually a continuous reduction in diffusion impedance with increasing temperature

is expected [47,56]. Possible causes could be transient effects during the heating phase, inhomogeneous temperature distributions within the cell, or measurement uncertainties that were not conclusively investigated within this work. Summarily, the heating and temperature control phase (Phase II) shows that aEIS delivers stable and consistent results even under changed thermal conditions. With increasing temperature, R_0 and R_{RQ} decrease, while C_Q increases. The model parameters agree well with the reference measurements, and the DRT analysis confirms the temperature-induced acceleration of electrochemical processes.

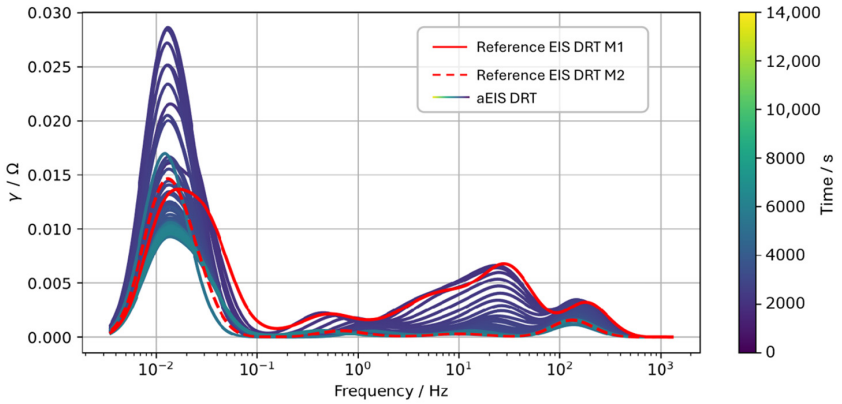

Figure 9. Comparison of DRT Analysis of aEIS and Reference Measurement from 2000 to 8000 s.

5.4. Phase III

In Phase III, after concluding the temperature control phase, the battery cell undergoes controlled cooling to examine the behavior of electrochemical parameters during decreasing temperatures. Starting at t = 8000 s, the heating mode of the climate chamber is deactivated, allowing the cell to gradually cool towards room temperature via continued active air circulation. The goal of this phase is to check whether aEIS delivers reliable measurement results during dynamic cooling processes and whether the electrochemical parameters show the expected temperature-dependent reversal. Figure 10a shows the Nyquist plot of the impedance measurements from 8000 to 15,000 s. During passive cooling, the impedance curves continuously shift to higher values. The diameter of the semicircle increases again, indicating an elevation in both ohmic resistance R_0 and charge-transfer-limited resistance R_{RQ}. This observation matches physical expectations, as with decreasing temperature, ion diffusion coefficients and reaction rates decline, reflected in an increase in overall impedance [44,53].

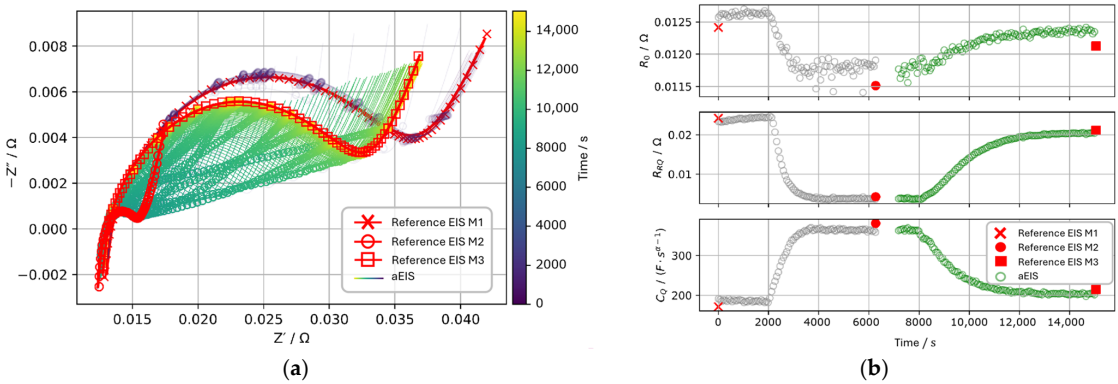

Figure 10. (**a**) Nyquist Plot of aEIS and Reference Measurement; (**b**) Temporal Evolution of Selected ECM Parameters from 8000 to 15,000 s.

The aEIS measurement results show very good agreement with the reference measurements, confirming the robustness and stability of the method even under dynamically varying thermal conditions.

Quantitative validation at matching frequency points confirms this visual agreement, showing a mean impedance magnitude deviation of 0.29% with a maximum of 0.62%. The temporal evolution of the modeled ECM parameters is depicted in Figure 10b. Both R_0 and R_{RQ} continuously increase during cooling, reflecting the temperature-dependent slowing of electrochemical reaction kinetics [44,53].

Notably, R_0 exhibits stronger scattering compared to R_{RQ}, indicating heightened sensitivity of the ohmic component to local temperature gradients and inhomogeneities within the cell. In contrast, the capacitance C_Q continuously decreases during the cooling phase, attributable to reduced ion dynamics and decreased effective double-layer capacitance at lower temperatures [53,56]. Overall, the model parameters extracted from aEIS measurements agree very well with the results of the reference measurements, confirming the validity and reproducibility of aEIS even during the cooling phase.

For further analysis, a DRT evaluation is performed, shown in Figure 11.

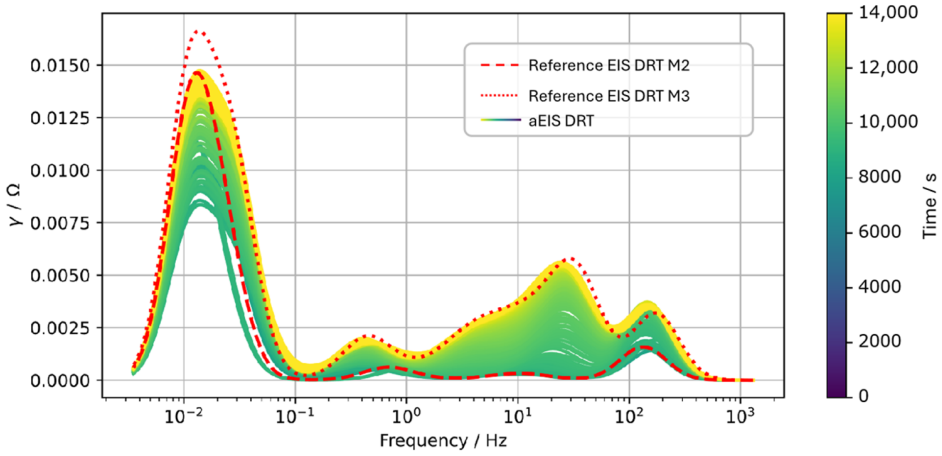

Figure 11. Comparison of DRT Analysis of aEIS and Reference Measurement from 8000 to 15,000 s.

The DRT representation shows a clear shift of the main relaxation peaks to longer relaxation times, reflecting the temperature-induced slowing of electrochemical processes. Additionally, an increase in resistive components of the relaxation peaks is noticeable in the mid-frequency range, indicating the rise in charge-transfer-limited and ohmic resistances as temperature decreases [47,48,56].

The calculated DRT courses of aEIS again match very well with the reference data, underscoring the high quality and consistency of the aEIS method even during the cooling phase. Notably, unlike the heating phase, no implausible changes in the low-frequency diffusion-limited peak occur. The diffusion-related components evolve continuously and without strong fluctuations throughout the cooling process, suggesting a more uniform thermal relaxation. Possibly, the slower temperature reduction through passive cooling contributes to stabilizing the diffusion-limited processes, avoiding transient artifacts observed during the dynamic heating phase.

Summarily, the cooling phase (Phase III) demonstrates that aEIS delivers valid results even during dynamic temperature drops. R_0 and R_{RQ} increase with decreasing temperature, while C_Q decreases. R_0 exhibits slightly higher scattering compared to R_{RQ}. The model parameters extracted from aEIS measurements agree very well with the reference data, and the DRT analysis confirms the temperature-dependent slowing of electrochemical relaxation processes. Thus, Phase III also corroborates the functionality and reliability of aEIS under dynamically decreasing temperatures.

6. Discussion

The aEIS presented in this work offers several advantages for use in dynamic applications such as battery-operated and FC-powered vehicles.

6.1. Advantages in Vehicle/Dynamic Operation

A key advantage of aEIS is the significant reduction in measurement time by approximately 92%, making the method particularly suitable for time-sensitive applications in vehicle operation. The measurement duration was experimentally validated to be reduced from originally 677 s to just 60 s. Despite this considerable reduction, aEIS showed high agreement with the reference measurements, enabling reliable characterization of electrochemical processes. Additionally, aEIS had no measurable influence on the electrochemical behavior of the cell, which renders the method fundamentally suitable for continuous application. The consistent modelability with the chosen ECM throughout the entire test period underscores the stability and reproducibility of the method under controlled conditions.

6.2. Significance of Reduced Measurement

The reduced number of measurement points in aEIS enables quick measurements without significant information loss. This was confirmed under laboratory conditions, where the method provided high methodological insight with simultaneous data reduction. However, the validity of aEIS in real operation remains to be proven, especially under dynamic loads, temperature gradients, and noise influences. Further tests under real driving conditions are necessary to confirm the robustness and reliability of the method in practice-oriented scenarios.

6.3. Compatibility with Battery Health Monitoring

The aEIS parameterization correlates closely with relevant state variables such as internal resistance, capacity, and diffusion. This indicates that the method is principally integrable into existing battery management systems. The proof-of-concept demonstrated that aEIS provides the necessary information to precisely monitor the battery SoH and provide prognostic statements about its lifespan.

6.4. Limitations and Possible Extensions

The experiments conducted so far were performed under idealized laboratory conditions that do not fully replicate real vehicle environments. Temperature gradients, vibrations, current pulses, and changes in contact resistance could affect the measurement results. Additionally, the method has only been validated for a narrow temperature and load range, and its behavior under transient states remains unclear. Aging validation is also lacking, leaving the long-term stability and the influence of progressive degradation unexplored. The current implementation was limited to single-cell experiments, restricting the transferability to modules or stacks. Nevertheless, the basic version of aEIS offers considerable potential for increasing efficiency and robustness through advanced adaptive frequency point selection and optimized temporal sampling. Monitoring frequency is crucial for prognostic modeling, especially for estimating remaining useful life and SoH. These models depend on temporal trends of degradation indicators, and the measurement frequency determines the density of available data points. Too infrequent monitoring may fail to capture degradation trends adequately, while excessive monitoring offers diminishing returns. Balancing the monitoring frequency is thus essential for obtaining reliable and actionable prognostic information.

Comparing infrequent versus frequent monitoring reveals distinct advantages and limitations. Infrequent monitoring, such as monthly checks, captures only coarse trends and

may delay the detection of accelerated degradation. In contrast, more frequent monitoring provides better trend resolution and enables earlier identification of deviations, facilitating proactive maintenance and enhanced system reliability.

In summary, our work shows that aEIS is a promising method for SoH monitoring of galvanic cells in dynamic applications. The results underscore the need for further research to validate the method under real conditions and confirm its applicability in practice.

7. Conclusions and Outlook

In this work, EIS has been examined as a central tool for determining the state of galvanic cells. EIS provides a detailed analysis of electrochemical processes and enables the identification of degradation mechanisms, making it an almost indispensable method. However, the long measurement durations and the need for stable system operation during the measurement pose significant challenges, especially for use in dynamic applications such as battery-operated and FC-powered vehicles.

By developing and validating an accelerated EIS method, the measurement duration can be significantly reduced without losing diagnostic insights. The aEIS utilizes model-supported parameter analyses and targeted frequency selection to precisely capture relevant electrochemical processes. Experimental results showed excellent agreement between aEIS measurements and reference data captured by a conventional EIS, both under stable and dynamically changing conditions.

The aEIS method offers several advantages for vehicle operation, including a significant reduction in measurement time, reliable characterization despite reduced measurement time, and the possibility of integration into existing battery or fuel cell management systems. Additionally, the reduction in measurement data allows for advanced degradation analysis techniques to be applied directly within the vehicle. Adaptive frequency reduction significantly enhances the feasibility of EIS under dynamic conditions. By decreasing the measurement duration, it mitigates the need for stable operating points, rendering EIS more viable in real-world, transient scenarios. Positioned as a complementary component, the proposed method augments dynamic EIS applications, providing valuable insights without the constraints imposed by protracted measurement times. These methods will enable continuous monitoring and prediction of cell degradation, enhancing overall system reliability and longevity. Further development steps aim to integrate these degradation analysis capabilities alongside the optimization of the presented procedure principle.

However, there are limitations and potential extensions, such as validation under real vehicle conditions, consideration of aging processes, and extension to more complex systems like battery modules or fuel cell stacks. While the primary focus has been on reducing the measurement duration of EIS to accommodate the dynamic operating conditions of vehicles, it would be worthwhile to investigate whether this approach could be adapted for EIS measurements conducted exclusively under operational loads over extended periods. In such a scenario, the model would necessarily need to incorporate aging processes to maintain accuracy and relevance. Such an adaptation could provide valuable insights into long-term degradation mechanisms and enhance strategic maintenance planning. Future research should explore this avenue to determine if integrating aging models into prolonged operational EIS measurements can offer complementary benefits to this accelerated EIS method.

While acknowledging the trade-off between time savings and potential loss of information, it is important to note that both EIS and aEIS datasets are available. However, the present work focuses on establishing the methodical proof-of-concept. A comprehensive quantitative comparison was not included to avoid extending the scope excessively and to preserve the readability and focus of the work. Quantitative validation, including metrics

such as root mean square error, parameter errors, and correlation coefficients, is planned for a follow-up study.

For the next developmental steps, an extensive measurement campaign is planned to further improve aEIS under realistic conditions. This also includes optimizing the model and adapting the measurement methodology to the specific requirements of fuel cells. Future research will also focus on the sensitivity analysis of the method, particularly the influence of various SoC (e.g., 20% to 80%) and different aging stages on the robustness of the procedure. Additional experiments are necessary to demonstrate the adaptability of the frequency selection strategy under changing parameters. Future research will also focus on the correlation of indicators or measurement parameters for determining the system state and their significance for degradation. Possible contributions from non-stationary operating conditions, internal thermal gradients, or other experimental factors will be considered.

The creation of time comparison data with different numbers of measurement points will also be carried out to investigate the interplay between the number of measurement points and time savings, thereby exploiting the potential for reducing measurement time based on an optimal measurement point density. In addition, the potential of supporting further EIS-independent measurement and modeling methods should also be tested to primarily strengthen synergies for the accuracy and predictability of the measurements.

Currently, the test phase of a short stack is underway, which already promises encouraging measurement data. With the goal of measuring both the battery and the fuel cells in an FC vehicle with minimal methodological and technical effort using aEIS, a modification of the existing DC-DC converter in the vehicle is ultimately envisaged. This would reduce the space requirement, cost, and weight of the additional measurement technology to a minimum. Such a modified DC-DC converter would be capable of recording accelerated impedance spectra in addition to its usual function as a voltage and current converter.

Transitioning from the controlled laboratory setting to the dynamic vehicular environment necessitates addressing several critical engineering constraints. Key considerations include stringent instrumentation requirements, such as four-wire/four-electrode measurements, robust shielding protocols, and galvanic isolation mechanisms. Furthermore, the operational integrity of the system under conditions of switching noise and electromagnetic interference must be meticulously managed. The feasibility of integrating aEIS through modifications to the DC-DC converter must be thoroughly assessed. The engineering constraints mentioned above present significant challenges. This requires a differentiated view of the technical challenge to realize the implementation at the vehicle level. Future research efforts should focus on bridging the gap between laboratory experiments and real-world applicability to ensure that the aEIS demonstrates resilience under the challenging conditions encountered in vehicular environments.

Author Contributions: Conceptualization, N.M. and S.E.; methodology, N.M. and S.E.; software, S.E.; validation, N.M. and S.E.; formal analysis, N.M. and S.E.; investigation, N.M. and S.E.; resources, N.M. and S.E.; data curation, N.M. and S.E.; writing—original draft preparation, N.M. and S.E.; writing—review and editing, N.M.; visualization, N.M. and S.E.; supervision, N.M.; project administration, N.M. All authors have read and agreed to the published version of the manuscript.

Funding: This research received no external funding.

Data Availability Statement: The original contributions presented in this study are included in the article. Further inquiries can be directed to the corresponding author.

Conflicts of Interest: The authors declare no conflicts of interest.

Abbreviations

The following abbreviations are used in this manuscript:

AC	Alternating Current
aEIS	accelerated Electrochemical Impedance Spectroscopy
CAN	Controller Area Network
CPE	Constant Phase Element
CVM	Cell Voltage Monitoring
DC	Direct Current
DRT	Distribution of Relexation Times
DLR	Deutsches Zentrum für Luft- und Raumfahrt (German Aerospace Center)
ECM	Equivalent Circuit Model
FC	Fuel Cell
EIS	Electrochemical Impedance Spectroscopy
KKT	Kramers-Kronig-Transformation
OCV	Open Circuit Voltage
PEM	Proton Exchange Membrane
SoC	State of Charge
SoH	State of Health
QSC	Quasi-Stationary Conditions

References

1. U.S Department of Energy. Energy Efficiency and Renewable Energy. Available online: https://www.energy.gov/sites/prod/files/2015/11/f27/fcto_fuel_cells_fact_sheet.pdf (accessed on 3 October 2025).
2. Sazali, N.; Salleh, W.; Jamaludin, A.S.; Razali, M. New Perspectives on Fuel Cell Technology: A Brief Review. *Membranes* **2020**, *10*, 99. [CrossRef] [PubMed]
3. Bortnowska, M.; Zmuda, A. A Comparative Analysis of Hydrogen Fuel Cells and Internal Combustion Engines Used for Service Operation Vessels Propulsion. *Energies* **2025**, *18*, 5104. [CrossRef]
4. Marcinkoski, J.; Vijayagopal, R.; Adams, J.; James, B.; Kopasz, J.; Ahluwalia, R. *Hydrogen Class 8 Long Haul Truck Targets*; DOE Hydrogen & Fuel Cells Program Record No. 19006; U.S. Department of Energy: Washington, DC, USA, 2019.
5. Ballard Power Systems, Inc. FCmove-XD v2—Data Sheet (04/2024). Available online: https://www.ballard.com/wp-content/uploads/2024/11/Ballard-Data-Sheet-FCmove-XDv2_20250305_landscape-2.pdf (accessed on 15 October 2025).
6. Paffumi, E.; De Gennaro, M.; Martini, G. European-wide study on big data for supporting road transport policy. *Case Stud. Transp. Policy* **2018**, *6*, 785–802. [CrossRef]
7. Meszler, D.; Hill, N.; Bannister, R.; Kelly, M. *Efficiency Technologies for Long-Haul Tractor-Trailers: EU HDV Tech Targets 2025–30*; The International Council on Clean Transportation: Washington, DC, USA, 2018.
8. Danielis, R.; Scorrano, M.; Masutti, M.; Awan, A.M.; Niazi, A.M.K. The Economic Competitiveness of Hydrogen Fuel Cell-Powered Trucks: A Review of Total Cost of Ownership Estimates. *Energies* **2024**, *17*, 2509. [CrossRef]
9. Kurtz, J.; Sprik, S.; Saur, G.; Onorato, S. *Fuel Cell Electric Vehicle Durability and Fuel Cell Performance*; NREL/TP-5400-73011; National Renewable Energy Laboratory: Golden, CO, USA, 2019. Available online: https://www.nrel.gov/docs/fy19osti/73011.pdf (accessed on 27 October 2025).
10. Wu, Q.; Dong, Z.; Zhang, X.; Zhang, C.; Iqbal, A.; Chen, J. Towards More Efficient PEM Fuel Cells Through Advanced Thermal Management: From Mechanisms to Applications. *Sustainability* **2025**, *17*, 943. [CrossRef]
11. Kordel, M. Innovative Metal Hydride Refrigeration System. In Proceedings of the ECS Simulation Conference 2023, Linz, Austria, 10–11 May 2023.
12. Muck, N.; Wieser, S.; Deniz, Ö.; Scharmach, M. Model-based Investigation and Evaluation of a Hydrogen Expansion Engine by Determining System Efficiency as Well as Market Development for Heavy-Duty Hydrogen Vehicles. In Proceedings of the 2nd International Conference on Sustainable Mobility Applications, Renewables and Technology (SMART 2022), Cassino, Italy, 23–25 November 2022. [CrossRef]
13. Rufer, A. Expansion Work Recovery of Hydrogen for a FC-Truck-Tentative Design of an Expansion Machine. *Preprints* **2023**, 2023061326. [CrossRef]
14. Muck, N.; Wieser, S. Analysis of Hydrogen Expansion Potential for Fuel Cell Electric Vehicles Efficiency. In Proceedings of the 16th International Conference on Ecological Vehicle and Renewable Energies (EVER 2021), Monte Carlo, Monaco, 5–7 May 2021. [CrossRef]

15. Andrade, P.; Laadjal, K.; Alcaso, A.N.; Cardoso, A.J.M. A Comprehensive Review on Condition Monitoring and Fault Diagnosis in Fuel Cell Systems: Challenges and Issues. *Energies* **2024**, *17*, 657. [CrossRef]
16. Knowles, M.; Baglee, D.; Morris, A.; Ren, Q. The State of the Art in Fuel Cell Condition Monitoring and Maintenance. *World Electr. Veh. J.* **2010**, *4*, 487–494. [CrossRef]
17. Mulder, G.; De Ridder, F.; Coenen, P.; Weyen, D.; Martens, A. Evaluation of an On-Site Cell Voltage Monitor for Fuel Cell Systems. *Int. J. Hydrogen Energy* **2008**, *33*, 5728–5737. [CrossRef]
18. Sutharssan, T.; Montalvao, D.; Chen, Y.K.; Wang, W.-C.; Pisac, C.; Elemara, H. A Review on Prognostics and Health Monitoring of Proton Exchange Membrane Fuel Cells. *Renew. Sustain. Energy Rev.* **2017**, *75*, 440–450. [CrossRef]
19. Tian, Q.; Chen, H.; Ding, S.; Shu, L.; Wang, L.; Huang, J. Remaining Useful Life Prediction Method of PEM Fuel Cells Based on a Hybrid Model. *Electronics* **2023**, *12*, 3883. [CrossRef]
20. Niu, W.; Li, X.; Tian, H.; Liang, C. Remaining Useful Life Prediction of PEMFC Based on 2-Layer Bidirectional LSTM Network. *World Electr. Veh. J.* **2025**, *16*, 511. [CrossRef]
21. Pan, H.; Zou, Y.; Sun, X.; Fu, J. An enhanced neural network model for predicting the remaining useful life of proton exchange membrane fuel cells. *Sci. Rep.* **2025**, *15*, 37320. [CrossRef] [PubMed]
22. Dirkes, S.C.; Pischinger, S.; Eichel, R.-A. Entwicklung eines fahrzeugbasierten präskriptiven Lebensdauermanagements zur degradationstoleranten Betriebsführung von PEM-Brennstoffzellensystemen. Ph.D. Thesis, Rheinisch-Westfälische Technische Hochschule Aachen, Aachen, Germany, 2025. [CrossRef]
23. Deiss, E. Spurious Chemical Diffusion Coefficients of Li^+ in Electrode Materials Evaluated with GITT. *Electrochim. Acta* **2005**, *50*, 2927–2932. [CrossRef]
24. Hallemans, N.; Howey, D.; Battistel, A.; Saniee, N.F.; Scarpioni, F.; Wouters, B.; La Mantia, F.; Hubin, A.; Widanage, W.D.; Lataire, J. Electrochemical Impedance Spectroscopy Beyond Linearity: A Comprehensive Review. *J. Electroanal. Chem.* **2023**, *101*, 1143–1156. [CrossRef]
25. Meyer, L.; Saqib, N.; Porter, J. Operando Optical Spectroscopy Studies of Batteries. *J. Electrochem. Soc.* **2021**, *168*, 090561. [CrossRef]
26. Su, L.; Xu, Y.; Dong, Z.Y. State-of-health estimation of lithium-ion batteries: A comprehensive literature review from cell to pack levels. *Energy Convers. Econ.* **2024**, *5*, 224–242. [CrossRef]
27. Tang, K.; Luo, B.; Chen, D.; Wang, C.; Chen, L.; Li, F.; Cao, Y.; Wang, C. The State of Health Estimation of Lithium-Ion Batteries: A Review of Health Indicators, Estimation Methods, Development Trends and Challenges. *World Electr. Veh. J.* **2025**, *16*, 429. [CrossRef]
28. Plett, G.L. *Battery Management Systems, Volume I: Battery Modeling*; Artech House: Norwood, MA, USA, 2015.
29. Wasylowski, D.; Ditler, H.; Sonnet, M.; Falkenstein, T.; Leogrande, L.; Ronge, E.; Blömeke, A.; Würsig, A.; Ringbeck, F.; Sauer, D.U. Operando Visualization of Lithium Plating by Ultrasound Imaging of Battery Cells. *Nat. Commun.* **2024**, *15*, 10237. [CrossRef]
30. Muck, N.; David, C.; Knöri, T. Integrating Fiber Sensing for Spatially Resolved Temperature Measurement in Fuel Cells. *Energies* **2024**, *17*, 16. [CrossRef]
31. Hu, X.; Li, S.; Peng, H. A Comparative Study of Equivalent Circuit Models for Li-Ion Batteries. *J. Power Sources* **2012**, *198*, 359–367. [CrossRef]
32. He, H.; Xiong, R.; Fan, J. Evaluation of Lithium-Ion Battery Equivalent Circuit Models for State of Charge Estimation by an Experimental Approach. *Energies* **2011**, *4*, 582–598. [CrossRef]
33. Remmlinger, J.; Buchholz, M.; Meiler, M.; Bernreuter, P.; Dietmayer, K. State-of-Health Monitoring of Lithium-Ion Batteries in Electric and Hybrid Vehicles. *J. Power Sources* **2011**, *196*, 10613–10620. [CrossRef]
34. Andre, D.; Meiler, M.; Steiner, K.; Wimmer, C.; Soczka-Guth, T.; Sauer, D.U. Characterization of High-Power Lithium-Ion Batteries by Electrochemical Impedance Spectroscopy. *J. Power Sources* **2011**, *196*, 5334–5341. [CrossRef]
35. Berecibar, M.; Gandiaga, I.; Villarreal, I.; Omar, N.; Van Mierlo, J.; Van den Bossche, P. Critical Review of State of Health Estimation Methods of Li-Ion Batteries. *Renew. Sustain. Energy Rev.* **2016**, *56*, 1342–1356. [CrossRef]
36. Yuan, X.-Z.; Zhang, S.; Wang, H.; Wu, J.; Sun, J.C.; Hiesgen, R.; Friedrich, K.A.; Schulze, M.; Haug, A. Degradation of a polymer exchange membrane fuel cell stack with Nafion® membranes of different thicknesses: Part I. In situ diagnosis. *J. Power Sources* **2010**, *195*, 7594–7599. [CrossRef]
37. Brunetto, C.; Moschetto, A.; Tina, G. PEM Fuel Cell Testing by Electrochemical Impedance Spectroscopy. *Electr. Power Syst. Res.* **2009**, *79*, 17–26. [CrossRef]
38. Wang, H.; Yuan, X.-Z.; Li, H. *PEM Fuel Cell Diagnostic Tools*; CRC Press: Boca Raton, FL, USA, 2012.
39. Padha, B.; Verma, S.; Mahajan, P.; Arya, S. Electrochemical Impedance Spectroscopy (EIS) Performance Analysis and Challenges in Fuel Cell Applications. *J. Electrochem. Sci. Technol.* **2022**, *13*, 167–176. [CrossRef]
40. Papula, L. *Mathematik für Ingenieure und Naturwissenschaftler*, 14th ed.; Springer Vieweg: Wiesbaden, Germany, 2015.
41. Wang, S.; Zhang, J.; Gharbi, O.; Vivier, V.; Gao, M.; Orazem, M. Electrochemical Impedance Spectroscopy. *Nat. Rev. Methods Primers* **2021**, *1*, 41. [CrossRef]
42. O'Hayre, R.; Cha, S.-W.; Colella, W.; Prinz, F.B. *Fuel Cell Fundamentals*, 3rd ed.; John Wiley & Sons: Hoboken, NJ, USA, 2016.

43. Meddings, N.; Heinrich, M.; Overney, F.; Lee, J.-S.; Ruiz, V.; Napolitano, E.; Seitz, S.; Hinds, G.; Raccichini, R.; Gaberšček, M.; et al. Application of electrochemical impedance spectroscopy to commercial Li-ion cells. *J. Power Sources* **2020**, *480*, 228742. [CrossRef]
44. Lasia, A. *Electrochemical Impedance Spectroscopy and Its Applications*; Springer: New York, NY, USA, 2014. [CrossRef]
45. Schönleber, M.; Klotz, D.; Ivers-Tiffée, E. A Method for Improving the Robustness of Linear Kramers-Kronig Validity Tests. *Electrochim. Acta* **2014**, *131*, 20–27. [CrossRef]
46. Boukamp, B.A. A Linear Kronig-Kramers Transform Test for Immittance Data Validation. *J. Electrochem. Soc.* **1995**, *142*, 1885–1894. [CrossRef]
47. Ivers-Tiffée, E.; Weber, A. Evaluation of electrochemical impedance spectra by the distribution of relaxation times. *J. Ceram. Soc. Jpn.* **2017**, *125*, 193–201. [CrossRef]
48. Gantenbein, S. Impedanzbasierte Modellierung von Lithium-Ionen Zellen und deren Degradationsverhalten. Ph.D. Thesis, KIT Scientific Publishing, Karlsruhe, Germany, 2019.
49. Lochner, T. Impedance Analysis and Monitoring of Automotive Fuel Cells. Ph.D. Thesis, Technische Universität München, Munich, Germany, 2021. Available online: https://mediatum.ub.tum.de/doc/1596139/1596139.pdf (accessed on 27 October 2025).
50. Hackmann, T.; Esser, S.; Danzer, M.A. Operando determination of lithium-ion cell temperature based on electrochemical impedance features. *J. Power Sources* **2024**, *615*, 235036. [CrossRef]
51. Haussmann, P.; Melbert, J. Internal Cell Temperature Measurement and Thermal Modeling of Lithium Ion Cells for Automotive Applications by Means of Electrochemical Impedance Spectroscopy. *SAE Int. J. Altern. Powertrains* **2017**, *6*, 261–270. [CrossRef]
52. Barsoukov, E.; Macdonald, J.R. *Impedance Spectroscopy: Theory, Experiment, and Applications*, 2nd ed.; Wiley: Hoboken, NJ, USA, 2005.
53. Jossen, A.; Weydanz, W. *Moderne Akkumulatoren Richtig Einsetzen*, 2nd ed.; MatrixMedia Verlag: Göttingen, Germany, 2021.
54. Wan, T.H.; Saccoccio, M.; Chen, C.; Ciucci, F. Influence of the Discretization Methods on the Distribution of Relaxation Times Deconvolution: Implementing Radial Basis Functions with DRTtools. *Electrochim. Acta* **2015**, *184*, 483–499. [CrossRef]
55. Tikhonov, A.; Goncharsky, A.; Stepanov, V.; Yagola, A.G. *Numerical Methods for the Solution of Ill-Posed Problems*; Springer Science & Business Media: Berlin/Heidelberg, Germany, 2013.
56. Schmidt, J.P. *Verfahren zur Charakterisierung und Modellierung von Lithium-Ionen Zellen*; KIT Scientific Publishing: Karlsruhe, Germany, 2013. [CrossRef]